in the imprinted sites, whereas predominantly aragonite was formed in solution, as expected. In some cases an occasional needle-like crystal of aragonite could be seen, which had probably been deposited onto the polymer particle during filtration and drying (compare Fig. 4e and g). More significantly, examination of the surface of control polymer **CP-2** (Fig. 4h) revealed the presence of deposited aragonite needles as well as a few sharp-edged 'solution-type' calcite crystals. A crystal-enriched fraction from **PI-1**, prepared by grinding and sedimentation in chloroform, was shown conclusively to contain calcite, both by FT-IR (Fig. 3b) and XRD (not shown).

We attempted to produce aragonite-specific polymers using the same monomer **1** and the needles shown in Fig. 4g as template. But the results of this experiment were inconclusive, as the polymers did not nucleate as well as those imprinted with calcite and neither FT-IR nor powder XRD were sensitive enough to quantify the ratio of aragonite to calcite on the polymer surface. It is not clear why the imprinting of calcite should result in much more efficient nucleation than the corresponding aragonite imprints. However, as the arrangement of ions on the crystal planes of each polymorph are different, it is reasonable to expect that a functionality which is suitable for creating complementary surfaces in one case may not necessarily be useful for another type of crystal. We note that the use of acrylic and methacrylic acids in place of the monomer **1** resulted in imprinted polymers with inferior nucleating abilities. The reason for this is not clear, but may be due to the presence of the flexible spacer which separates the acid head group from the polymerizable double bond of **1**, allowing this monomer to match more easily the spacing of ions on the crystal surface and for this ordering to be preserved throughout the entire imprinting process. Better understanding of these processes may enable the design of devices for generating crystals of the desired type, size or shape for applications in materials science. In addition, the ability to generate surfaces specific to crystals of an enantiomerically pure organic compound—to promote its crystallization from a racemic mixture—may lead to the introduction of new separation methods in the pharmaceutical and fine-chemical industries. □

Received 10 August 1998; accepted 13 January 1999.

1. Mann, S. Molecular recognition in biomineralization. *Nature* **332,** 119–124 (1988).
2. Berman, A. *et al.* Intercalation of sea-urchin proteins in calcite—study of a crystalline composite-material. *Science* **250,** 664–667 (1990).
3. Mann, S. Molecular tectonics in biomineralization and biomimetic materials chemistry. *Nature* **365,** 499–505 (1993).
4. Falini, G., Albeck, S., Weiner, S. & Addadi, L. Control of aragonite or calcite polymorphism by mollusk shell macromolecules. *Science* **271,** 67–69 (1996).
5. Mann, S., Heywood, B. R., Rajam, S. & Birchall, J. D. Controlled crystallization of $CaCO_3$ under stearic-acid monolayers. *Nature* **334,** 692–695 (1988).
6. Bianconi, P. A., Lin, J. & Strzelecki, A. R. Crystallization of an inorganic phase controlled by a polymer matrix. *Nature* **349,** 315–317 (1991).
7. Bunker, B. C. *et al.* Ceramic thin-film formation on functionalized interfaces through biomimetic processing. *Science* **264,** 48–55 (1994).
8. Walsh, D. & Mann, S. Fabrication of hollow porous shells of calcium carbonate from self-organizing media. *Nature* **377,** 320–323 (1995).
9. Oliver, S., Kuperman, A., Coombs, N., Lough, A. & Ozin, G. A. Lamellar aluminophosphates with surface patterns that mimic diatom and radiolarian microskeletons. *Nature* **378,** 47–50 (1995).
10. Berman, A. *et al.* Total alignment of calcite at acidic polydiacetylene films—cooperativity at the organic-inorganic interface. *Science* **269,** 515–518 (1995).
11. Mann, S. & Ozin, G. A. Synthesis of inorganic materials with complex form. *Nature* **382,** 313–318 (1996).
12. Ozin, G. A. Morphogenesis of biomineral and morphosynthesis of biomimetic forms. *Acc. Chem. Res.* **30,** 17–27 (1997).
13. Yang, H., Coombs, N. & Ozin, G. A. Morphogenesis of shapes and surface patterns in mesoporous silica. *Nature* **386,** 692–695 (1997).
14. Küther, J., Seshadri, R., Knoll, W. & Tremel, W. Templated growth of calcite, vaterite and aragonite crystals on self-assembled monolayers of substituted alkylthiols on gold. *J. Mater. Chem.* **8,** 641–650 (1998).
15. Ozin, G. A. *et al.* Bone mimetics: A composite of hydroxyapatite and calcium dodecylphosphate lamellar phase. *J. Mater. Chem.* **7,** 1601–1607 (1997).
16. Heywood, B. R. & Mann, S. Template-directed nucleation and growth of inorganic materials. *Adv. Mater.* **6,** 9–20 (1994).
17. Wulff, G. Molecular imprinting in cross-linked materials with the aid of molecular templates—a way towards artificial antibodies. *Angew. Chem. Int. Edn Engl.* **34,** 1812–1832 (1995).
18. Mosbach, K. & Ramström, O. The emerging technique of molecular imprinting and its future impact on biotechnology. *Bio/Technology* **14,** 163–170 (1996).
19. Shea, K. J. Molecular imprinting of synthetic network polymers: The *de novo* synthesis of macromolecular binding and catalytic sites. *Trends Polym. Sci.* **2,** 166–173 (1994).
20. Vulfson, E. N., Alexander, C. & Whitcombe, M. J. Assembling the molecular cast. *Chem. Brit.* **33,** 23–26 (1997).
21. De Keyser, W. L. & Degueldre, L. Contribution à l'étude de la formation de la calcite, aragonite et vaterite. *Bull. Soc. Chim. Belg.* **59,** 40–71 (1950).
22. Reddy, M. M. & Nancollas, G. H. The crystallization of calcium carbonate IV. The effect of magnesium, strontium and sulfate ions. *J. Cryst. Growth.* **35,** 33–38 (1976).
23. Batz, H.-G. & Koldehoff, J. Monomere und polymere succinimidoester von ω-methacryloylamino-säuren, ihre darstellung und ihre reaktion mit aminen. *Makromol. Chem.* **177,** 683–686 (1976).

Acknowledgements. We thank A. Jahans for the X-ray crystallographic studies. This work was supported by BBSRC and Unilever plc.

Correspondence and requests for materials should be addressed to M.J.W. (e-mail: michael.whitcombe@bbsrc.ac.uk).

Ubiquity of quasi-horizontal layers in the troposphere

Reginald E. Newell*, Valerie Thouret*†, John Y. N. Cho*, Patrick Stoller*‡, Alain Marenco† & Herman G. Smit§

** Department of Earth, Atmospheric and Planetary Sciences, Massachusetts Institute of Technology, Cambridge, Massachusetts 02139, USA*
† Laboratoire d'Aerologie (CNRS-URA OMP 0354), F-31400 Toulouse, France
§ Research Center Jülich, Institute for Chemistry of the Polluted Atmosphere (ICG-2), PO Box 1913, 52425 Jülich, Germany

Fine laminar structures in the atmosphere have been described previously[1–9], but their characterization has been limited. The modern global coverage of aircraft flights offers an opportunity to provide such a characterization, and examine the ubiquity of such structures, in space and time. Research aircraft measuring vertical profiles of atmospheric chemical constituents frequently discern quasi-horizontal atmospheric layers with mean thicknesses of the order of 1 km and mean altitudes between 5 and 7 km (refs 10–12). These layers can be characterized and categorized by various combinations of ozone, water vapour, carbon monoxide and methane deviations from background profiles. Five commercial aircraft have been recently equipped to measure water vapour and ozone concentrations, and automatically collect vertical profile information on landing and take-off (refs 13–15). Here we synthesize measurements from both research and commercial flights and demonstrate the ubiquity in space and time of four layer types (as categorized by their chemical signatures). Up to one-fifth of the lowest 12 km of the atmosphere is occupied by such layers. We suggest that this universality reflects basic characteristics of the atmosphere hitherto unexplored, with potential implications for present understanding of a wide variety of dynamic and chemical atmospheric processes.

Atmospheric vertical structure has traditionally been measured with temperature and water-vapour sensors on balloon-borne radiosondes rising at about $5\,m\,s^{-1}$. The balloon is tracked to provide wind data. Although data can be collected at 6-s intervals, they are generally only reported at height intervals of 1.5–2.5 km, so a climatology of smaller-scale atmospheric structure is not available. Research aircraft measure many different atmospheric trace constituents while carrying out studies of ozone and other trace constituent budgets, providing a more precise identification of atmospheric layers. In addition, five Airbus A-340 aircraft in regular commercial service now measure ozone[13,14] and water vapour[14,15] continuously in flight, covering a substantial geographical area (the "MOZAIC" programme). Each time these aeroplanes take off and land an atmospheric vertical profile is traced out. We have used aircraft data from MOZAIC and three NASA missions: Pacific Exploratory Mission-West A (PEMA), in the western Pacific, September–October 1991; PEM-West B (PEMB), February–March 1994; and PEM-Tropics (PEMT), in the central and South

‡ Present address: Lawrence Livermore National Laboratory, 7000 East Avenue, Livermore, California 94550, USA.

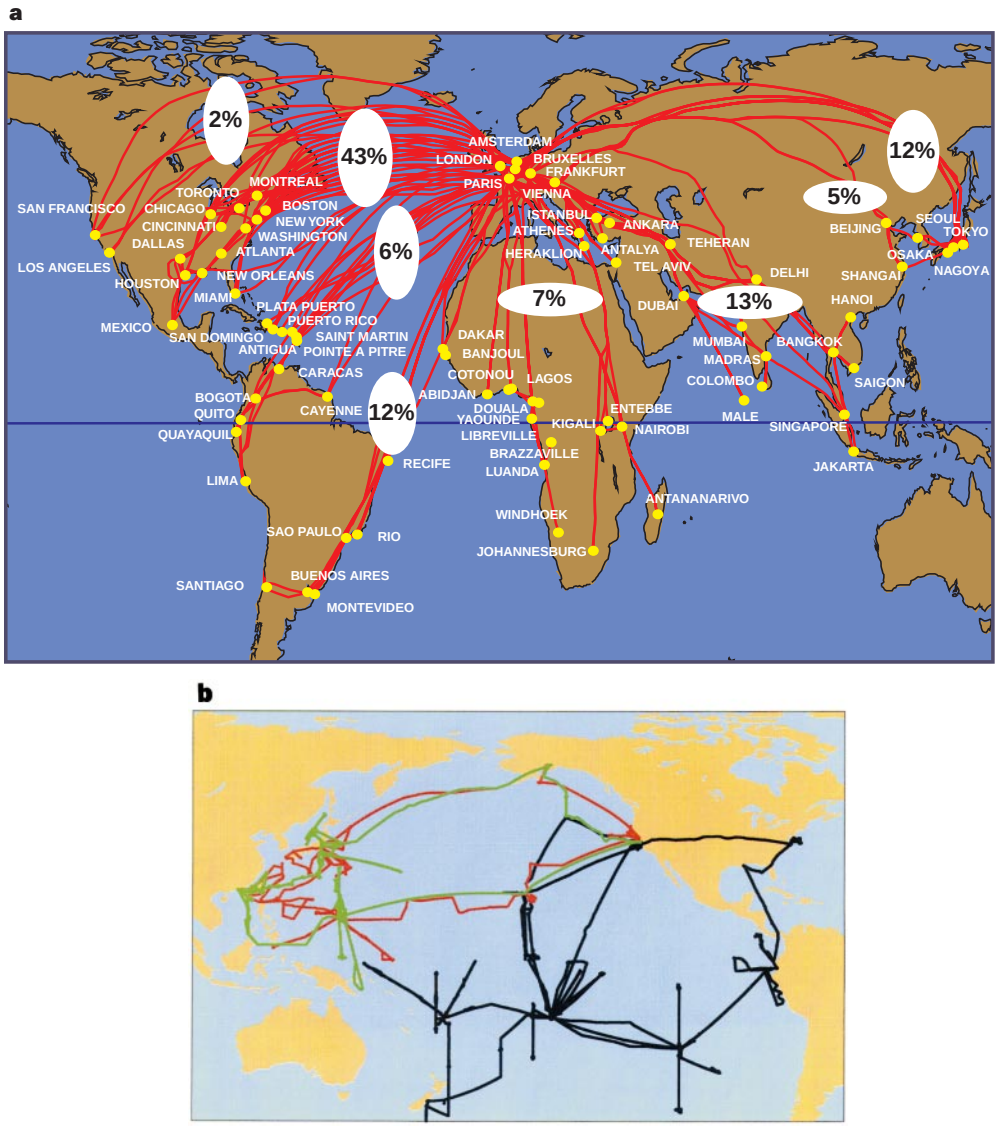

Figure 1 Maps of regions sampled. **a**, MOZAIC flight track and percentage of total flights (7,500) in indicated regions, September 1994–December 1997. Vertical profiles were only collected on take-off and landing. **b**, PEM flight tracks for 64 flights. Red, PEMA; green, PEMB; black, PEM tropics. Vertical profiles were collected throughout each flight.

Pacific, September–October 1996. Descriptions of PEMA, PEMB and PEMT with flight plans, instrument information and scientific findings, including layer examples and statistical summaries, are available[10–12,16–18]; MOZAIC and PEM coverages are shown in Fig. 1. MOZAIC is clearly more extensive; three full years of data are used here and the programme continues, while PEM was limited to the six months listed above. Comparison with the MOZAIC data thus provides a broader perspective on small-scale structure.

For each constituent profile, we estimated a background using a mode-based algorithm[12]. We characterized layers by calculating deviations from this background profile. The points with deviations of ±10 parts per billion by volume (p.p.b.v.) for O_3 and ±5% for water vapour as relative humidity were defined as layers. Ozone was examined first, then water vapour; if both exceeded these limits, we defined a layer. Layer thickness was determined by finding the nearest points where the ozone deviation was below 5 p.p.b.v. in magnitude. For the research aircraft data, CO and CH_4 were also included, with deviations of ±3 p.p.b.v., to define a second set of layers for which all four criteria were exceeded[12]. The much larger MOZAIC data sample permitted exploring variations in the magnitudes of the criteria for a layer from 5 p.p.b.v. to 20 p.p.b.v. for ozone and 5% to 20% for water vapour. To identify the layers, deviations from background are henceforth indicated by plus and minus signs following the chemical symbol: O_3+/H_2O– labels a layer characterized by a positive deviation from the background ozone profile coupled with a negative deviation from the background water-vapour profile. Results (Table 1) show increases in the number of layers for the smaller criteria. Average thicknesses of the layers are between 0.5 and 1.3 km and average altitudes are between 5.5 and 6.6 km.

A preliminary interpretation of the four combinations, based on the research aircraft data, is: O_3+/H_2O+, continental pollution; O_3+/H_2O–, stratospheric air or pollution; O_3–/H_2O+, convection from the boundary layer; and O_3–/H_2O–, subsiding air originally raised in deep convection over oceans. The properties of the different types vary with the anomaly criteria selected. The average altitude decreases as the criterion for water-vapour anomaly increases, while larger ozone anomalies yield higher altitudes for O_3+. Table 2a shows the universality in percentage distribution of the four layer types between the research aircraft and MOZAIC samples for O_3 ± 10 p.p.b.v. and relative humidity ±5%, despite geographical coverage and seasonal differences. The O_3+/H_2O– layer type is always the most abundant. For the same criteria, Table 2b shows that the mean heights of the different layer types

vary over a small range, while the thicknesses in PEMT are the smallest overall, probably a result of the higher data resolution during PEMT[12]. From the total layer number for each sample set in Table 2b, their average thickness, and the vertical span sampled (Table 2c), we calculate that about 15% of the atmosphere is occupied by layers. For MOZAIC, this value diminishes to 7% if the large O_3 anomaly criterion (20 p.p.b.v.) is used, or to 8% if the large H_2O anomaly criterion (20%) is used. Use of four layer criteria enables the O_3+/H_2O– layers to be subdivided into those with stratospheric origins and those from pollution, as the former always have low concentrations of CO and usually low CH_4. However, the subdivision is complicated by the fact that high stability often accompanies stratospheric air in the troposphere and tends to trap pollutants. The conclusion that this type of layer is always the most abundant could only have been made with the extensive time and space coverage of MOZAIC; it reflects the fact that the transfer of stratospheric air into the troposphere is important in the atmospheric general circulation.

Danielsen long ago stressed the laminar structure of the atmosphere[1]; he was concerned with how radioactive debris injected into the stratosphere moved back into the troposphere[2]. He pointed out that atmospheric fine structure was omitted in normal reporting of balloon-borne radiosonde data and gave examples of how the structure could be recovered by reprocessing. Corby[3] and others[4–6] also used radiosonde data to study tropospheric Fine structure, while Sawyer[7] extended the work to the lower stratosphere using a radar-sonde theodolite. Fine structure of the 17–70 km region was also examined by tracking rocket-launched falling spheres by radar[8]. More recently, powerful clear-air radars have enabled wind and turbulence layers to be measured throughout the atmosphere[9]. Except for Danielsen the general interpretation of this work was that the layers were evidence of gravity waves. These waves are associated with wind velocity changes and some are thought to be orographically forced. But in the layers revealed by trace constituent measurements, there are often no wind velocity signatures evident[11]. Furthermore, the extensive MOZAIC observations show such structure over both land and sea, and frequently in regions where orographic forcing is absent.

Layers identified as continental pollution and marine boundary layer convection move upwards near their source regions, whereas stratospheric layers and clean marine air generally subside. Subsidence is particularly effective for layers drier than the background environment, as radiative effects give relative cooling near the layer base which tends to move the base downwards independently of any large-scale subsidence[12]. Radiative heating rate calculations for an O_3–/H_2O+ layer in the upper troposphere, using a standard radiative transfer program[19], give heating near the base and cooling near the top (Fig. 2) which yields a tendency towards destabilization. Such layers would be likely regions for the occurrence of clear air turbulence.

Table 1 MOZAIC layer data

Minimum H_2O deviation, 5%

	Min. O_3 dev.			
	5 p.p.b.v.	10 p.p.b.v.	15 p.p.b.v.	20 p.p.b.v.
Number				
O_3+/H_2O+	8,658	3,341	1,676	977
O_3+/H_2O–	20,771	11,288	6,703	4,327
O_3–/H_2O+	10,634	3,751	1,411	672
O_3–/H_2O–	11,284	4,000	1,457	657
Thickness (m)				
O_3+/H_2O+	475	679	927	1,083
O_3+/H_2O–	689	867	1,135	1,358
O_3–/H_2O+	515	779	1,113	1,313
O_3–/H_2O–	494	736	1,072	1,353
Height (m)				
O_3+/H_2O+	5,952	6,321	6,472	6,653
O_3+/H_2O–	5,543	5,735	5,888	6,042
O_3–/H_2O+	5,753	5,872	5,830	5,657
O_3–/H_2O–	5,855	5,994	6,100	6,093

Minimum O_3 deviation, 10 p.p.b.v.

	Min. H_2O dev.			
Number	5%	10%	15%	20%
O_3+/H_2O+	3,341	2,323	1,605	1,075
O_3+/H_2O–	11,288	8,846	6,656	5,266
O_3–/H_2O+	3,751	2,776	2,009	1,408
O_3–/H_2O–	4,000	2,706	1,829	1,343
Thickness (m)				
O_3+/H_2O+	679	710	739	719
O_3+/H_2O–	867	907	940	969
O_3–/H_2O+	779	795	804	820
O_3–/H_2O–	736	743	755	751
Height (m)				
O_3+/H_2O+	6,321	6,142	5,965	5,805
O_3+/H_2O–	5,735	5,637	5,571	5,478
O_3–/H_2O+	5,872	5,730	5,587	5,512
O_3–/H_2O–	5,994	5,900	5,837	5,780

These data are for August 1994–December 1997.

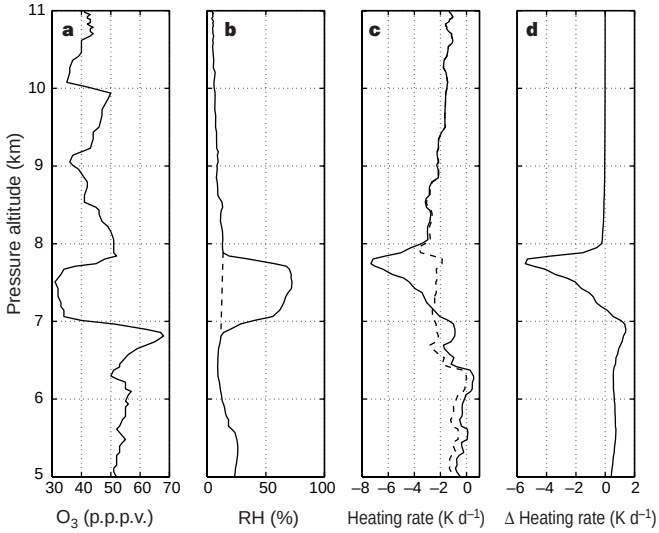

Figure 2 Radiative heating rate profiles for an O_3–/H_2O+ layer versus a simulated background, both without clouds. The data were obtained during a MOZAIC flight landing in Osaka on 12 November 1996, 00:25 UT. **a**, Ozone profile. **b**, Measured (solid line) and interpolated background (dashed) relative humidity (RH) profiles. The latter simulates a layerless situation. **c**, Calculated heating rate profiles for the measured RH (solid) and the interpolated layerless situation (dashed). **d**, Heating rate for the actual data minus the heating rate for the simulated background.

Table 2 Occurrence and characteristics of atmospheric layers

(a) Percentages of layer types for MOZAIC* and PEM

	O_3+/H_2O+	O_3+/H_2O–	O_3–/H_2O+	O_3–/H_2O–
PEMA	14	54	15	18
PEMB	11	54	17	18
PEMT	12	53	19	17
MOZAIC	15	50	17	18

(b) Number, thickness and height for layer types

	O_3+/H_2O+			O_3+/H_2O–			O_3–/H_2O+			O_3–/H_2O–		
	No.	Th.†	H.†	No.	Th.†	H.†	No.	Th.†	H.†	No.	Th.†	H.†
PEMA	11	0.68	5.7	43	0.76	5.2	12	0.87	5.1	14	0.86	6.5
PEMB	8	0.59	6.5	38	0.99	6.0	12	0.64	6.0	13	0.49	6.4
PEMT	27	0.45	6.0	120	0.71	5.2	43	0.47	5.4	38	0.45	6.1
MOZAIC	3,341	0.67	6.3	11,288	0.86	5.7	3,751	0.78	5.8	4,000	0.74	5.9

(c) Percentage of atmosphere occupied by layers

	Profiles‡ (km)	Avg. thickness (km)	Total no. of layers	% occupied
PEMA	439	0.78	80	14
PEMB	388	0.79	71	14
PEMT	655	0.59	228	20
MOZAIC	105,498	0.79	22,380	17

* From Table 1, upper section, O_3 ± 10 p.p.b.v.
† Thickness (Th.) and height (H.) in km.
‡ Total vertical distance sampled.

The relative invariance of percentages in Table 2a may reflect the overall mass balance that must occur. While the layers measured are mostly natural, some of the layers induced by biomass burning are from fires set by humans. Thus some anthropogenic effect on the buoyancy over the continents exists; this will be reflected elsewhere in more subsidence.

Atmospheric layers apparently play a significant role in the large-scale general circulation, in addition to the stratosphere–troposphere exchange noted above. Much upward motion in the atmosphere occurs via large-scale convergence in the lower atmosphere, followed by deep convection. This often culminates in a layer formed as the convected air spreads laterally in the upper troposphere. Upward motion also occurs in cyclones, and is often itself a quasi-horizontal layer-type process. Clouds are manifestations of these upward motions. The sinking motion which must accompany these processes is not always so evident. Dynamical and chemical numerical models used for weather forecasting, chemical-species time evolution and studies of climatic fluctuations should use a vertical resolution that is sufficient to define layers. Such resolution would be about 0.2 km or better, according to our observations—much higher than present-day models. The desired resolution for chemical models, in which highly nonlinear relationships are involved in ozone production[20], may be higher[21]. To accompany the enhanced resolution, the models will need to contain a new or modified formalism to include laminae.

When layers are included in atmospheric diagnostic and modelling studies, there are consequences for the mass, momentum and energy budgets. For example, layers of stratospheric air can be followed in the troposphere and their contribution to mass and trace-constituent exchange between the regions estimated. Another example is that the radiative cooling from layers rich in water vapour in the upper troposphere is substantially different from that of an upper troposphere with uniformly mixed water vapour (Fig. 2). The vertical gradients of cooling tend to produce instability which will influence the vertical energy and mass transport. A practical consequence is that clear air turbulence (CAT) could be triggered in such regions. Studies could be made of the occurrence of CAT near water vapour layers at high altitude such as those observed by MOZAIC; if there turned out to be an association, the layers could eventually be observed regularly with modified satellite limb scanning instruments. These have been used to delineate the upper-tropospheric water-vapour field and give results consistent with the large-scale atmospheric divergence field[22]. To detect the smaller-scale circulation features, the modifications would need to improve the vertical and horizontal resolution. □

Received 21 September 1998; accepted 7 January 1999.

1. Danielsen, E. F. The laminar structure of the atmosphere and its relation to the concept of a tropopause. *Arch. Meteorol. Geophys. Bioklimatol.* **11,** 293–332 (1959).
2. Danielsen, E. F. Stratospheric–tropospheric exchange based on ozone and potential vorticity. *J. Atmos. Sci.* **25,** 502–518 (1968).
3. Corby, G. A. A preliminary study of atmospheric waves using radiosonde data. *Q. J. R. Meteorol. Soc.* **83,** 49–60 (1957).
4. Reid, S. J. An observational study of lee waves using radiosonde data. *Tellus* **24,** 593–596 (1982).
5. Shutts, G. J., Kitchen, M. & Hoare, P. H. A large amplitude gravity wave in the lower stratosphere detected by radiosonde. *Q. J. R. Meteorol. Soc.* **114,** 579–594 (1988).
6. Bethan, S., Vaughan, G. & Reid, S. J. A comparison of ozone and thermal tropopause heights and the impact of tropopause definition on quantifying the ozone content of the troposphere. *Q. J. R. Meteorol. Soc.* **122,** 929–944 (1996).
7. Sawyer, J. S. Quasi-periodic wind variations with height in the lower stratosphere. *Q. J. R. Meteorol. Soc.* **87,** 24–33 (1961).
8. Newell, R. E., Mahoney, J. R. & Lenhard, R.. W. Jr A pilot study of small-scale wind variations in the stratosphere and mesosphere. *Q. J. R. Meteorol. Soc.* **92,** 41–54 (1966).
9. Gage, K. S. & Balsley, B. B. MST radar studies of wind and turbulence in the middle atmosphere. *J. Atmos. Terr. Phys.* **46,** 739–753 (1984).
10. Newell, R. E. *et al.* Vertical fine-scale atmospheric structure measured from NASA DC-8 during PEM-West A. *J. Geophys. Res.* **101,** 1943–1960 (1996).
11. Wu, Z.-X. *et al.* Atmospheric layers measured from the NASA DC-8 during PEM-West B and comparison with PEM-West A. *J. Geophys. Res.* **102,** 28353–28365 (1997).
12. Stoller, P. *et al.* Measurements of atmospheric layers from the NASA DC-8 and P-3B aircraft during PEM-Tropics A. *J. Geophys. Res.* (in the press).
13. Thouret, V., Marenco, A., Logan, J. A., Nédélec, P. & Grouhel, C. Comparisons of ozone measurements from the MOZAIC airborne program and the ozone sounding network at eight locations. *J. Geophys. Res.* **103,** 25695–25720 (1998).
14. Marenco, A. *et al.* Measurement of ozone and water vapour by Airbus in-service aircraft: The MOZAIC airborne program, an overview. *J. Geophys. Res.* **103,** 25631–25642 (1998).
15. Helten, M. *et al.* Calibration and performance of automatic compact instrumentation for the measurement of relative humidity from passenger aircraft. *J. Geophys. Res.* **103,** 25643–25652 (1998).
16. Hoell, J. M. *et al.* Pacific exploratory mission-west A (PEM-West A): September–October 1991. *J. Geophys. Res.* **101,** 1641–1653 (1996).
17. Hoell, J. M. *et al.* The Pacific exploratory mission-west phase B: February–March, 1994. *J. Geophys. Res.* **102,** 28223–28239 (1997).
18. Hoell, J. M. *et al.* The Pacific exploratory mission in the tropical Pacific: PEM-Tropics A, August–September, 1996. *J. Geophys. Res.* (in the press).
19. Hoffman, R. N. *A Computer Program which Calculates Radiative Fluxes and Heating Rates in Model Atmospheres* (Sci. Rep. No. 4, Dept Meteorol. Phys. Oceanogr., MIT, Cambridge, MA, 1981).
20. Brasseur, G P., Müller, J. F. & Granier, C. Atmospheric impact of NO_x emissions by subsonic aircraft: A three dimensional model study. *J. Geophys. Res.* **101,** 1423–1428 (1996).
21. Edouard, S., Legras, B., Lefevre, F. & Eymard, R. The effect of small-scale inhomogeneities on ozone depletion in the Arctic. *Nature* **384,** 444–447 (1996).
22. Newell, R. E., Zhu, Y., Browell, E. V., Read, W. G. & Waters, J. W. Walker circulation and tropical upper tropospheric water vapor. *J. Geophys. Res.* **101,** 1961–1974 (1996).

Acknowledgements. We thank our PEM and MOZAIC colleagues for access to their data, Air France, Lufthansa, Austrian Airlines and Sabena for carrying the MOZAIC equipment, and the NASA GTE, ACMAP, and GSFC Research Assistantship programs for their support.

Correspondence and requests for materials should be addressed to R.E.N. (e-mail: newell@newell1.mit.edu).